

Custom Coordination Environments for Lanthanoids: Tripodal Ligands Achieve Near-Perfect Octahedral Coordination for Two Dysprosium-Based Molecular Nanomagnets

Kwang Soo Lim,^{†,§} José J. Baldoví,^{‡,§} ShangDa Jiang,^{⊥,||,§} Bong Ho Koo,[†] Dong Won Kang,[†] Woo Ram Lee,[†] Eui Kwan Koh,[¶] Alejandro Gaita-Ariño,^{*,‡,§} Eugenio Coronado,[‡] Michael Slota,[⊥] Lapo Bogani,^{*,⊥} and Chang Seop Hong^{*,†,§}

[†]Department of Chemistry, Korea University, Seoul 136-713, Republic of Korea

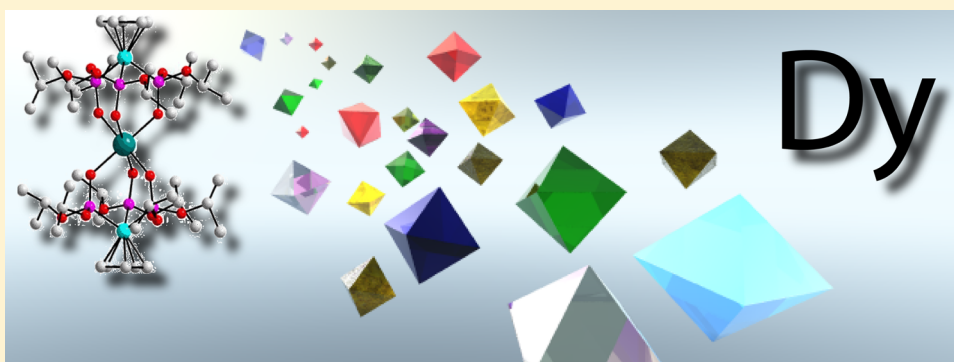
[‡]Instituto de Ciencia Molecular, Universidad de Valencia, C/Catedrático José Beltrán 2, Paterna E-46980, Spain

[⊥]Department of Materials, University of Oxford, 16 Parks Road, Oxford OX1 3PH, U.K.

^{||}Inorganic Chemistry, College of Chemistry and Molecular Engineering, Peking University, Beijing 100871, P. R. China

[¶]Nano-Bio System Research Team, Korea Basic Science Institute, Seoul 136-713, Korea

S Supporting Information



ABSTRACT: Controlling the coordination sphere of lanthanoid complexes is a challenging critical step toward controlling their relaxation properties. Here we present the synthesis of hexacoordinated dysprosium single-molecule magnets, where tripodal ligands achieve a near-perfect octahedral coordination. We perform a complete experimental and theoretical investigation of their magnetic properties, including a full single-crystal magnetic anisotropy analysis. The combination of electrostatic and crystal-field computational tools (SIMPRES and CONDON codes) allows us to explain the static behavior of these systems in detail.

INTRODUCTION

Since the first observation of slow magnetic relaxation in mononuclear lanthanide complexes $[\text{Pc}_2\text{Ln}]^-$ (Pc = phthalocyanide; Ln^{III} = Tb, Dy, Ho),¹ the field of mononuclear single-molecule magnets (SMMs) and molecular spin qubits has expanded significantly and now includes multiple examples based on either lanthanoids or transition metals, or even actinoids.² Considered to be classical bistable systems, they have set record values for the temperatures at which slow relaxation of the magnetization sets in. More interestingly, their quantum properties make them very attractive as spin qubit systems.³ Recently, record relaxation times have been obtained in transition-metal complexes, where there is a greater control over the coordination sphere.⁴ Moreover, in the quest for longer relaxation times at higher temperatures, different authors are now insisting on the need for exerting some control over the molecular vibrations and not only focusing on the thermal barrier.^{2b,5} The physics behind these arguments shares common

ground for both transition-metal and lanthanoid complexes, but chemical control of the coordination sphere is different. This is primarily due to the differences between the d and f orbitals (the latter being more internal) and secondarily due to the larger coordination spheres and higher coordination numbers of the lanthanoids. Attempts to address this problem have been performed by the use of rigid and bulky ligands such as polyoxometalates.⁶ Still, full validation of the theoretical models and the creation of a common background that can relate the rare-earth magnetism to the ligand-field analysis are largely unexplored.⁷

Dysprosium(III), in particular, has seen much use in the design of single-molecule magnets (SMMs) because of its high magnetic anisotropy.⁸ In sandwich-type structures, dysprosium(III) complexes should theoretically display strong axial

Received: December 21, 2016

anisotropy along the sandwich axis, but experiments show substantial deviations from these predictions. Despite insight obtained from octacoordinated dysprosium complexes with square-antiprismatic geometries, where the properties can be adjusted by local symmetry distortions and ligand substitution,⁹ the lack of model systems and of treatable situations is substantial. It has also been noted that special symmetries such as the octahedron or cube can give rise to unique quantum properties. As discussed previously by Baldoví et al.,¹⁰ the abundance of degenerate or near-degenerate electronic spin energy levels, even prior to the consideration of nuclear spins, creates a wealth of opportunities for avoided crossings and therefore for clock transitions (CTs), which can be used for improved quantum coherence, as we illustrated recently.¹¹ Furthermore, even in the absence of CTs, a sufficiently large number of spin states in an accessible energy window can be used to construct multiqubit (or d-bit) systems, where coherent transitions are demonstrated.¹²

Compared to dysprosium-based magnetic systems with coordination numbers larger than 7, a hexacoordinated dysprosium complex (not cluster) is rarely known^{13,14} and highly sought after to further understand fundamental magnet-like behaviors. Here we present the synthesis, structure, and magnetic properties of Dy SMMs in custom-shaped and uncommon octahedral coordination, providing model compounds for the understanding of rare-earth magnetism.

MATERIALS AND METHODS

Reagents. All chemicals and solvents in the synthesis were of reagent-grade and were used as received. Na[CpCo{P(O)(OEt)₂}₃] (NaL_{OEt}) and Na[CpCo{P(O)(OiPr)₂}₃] (NaL_{OiPr}) were prepared according to literature procedures.¹⁵

[Dy(L_{OEt})₂](PF₆) (**1**). NaL_{OEt} (55.7 mg, 0.10 mmol) and NH₄PF₆ (16.3 mg, 0.10 mmol) were dissolved in water (15 mL) and stirred for 10 min. A yellow precipitate was generated immediately upon the addition of Dy(NO₃)₃·5H₂O (17.4 mg, 0.05 mmol) in water (2 mL) to the ligand solution. The mixture was stirred for 12 h, and the precipitate was filtered and washed with water. Vapor diffusion of diethyl ether into a methanol solution yielded crystals suitable for X-ray analysis. Yield: 52.1 mg (75.6%). Anal. Calcd for C₃₄H₇₀Co₂DyF₆O₁₈P₇: C, 29.62; H, 5.12. Found: C, 29.62; H, 5.04.

[Y(L_{OEt})₂](PF₆). The yttrium analogue was obtained by the same procedure as that for compound **1**, except that Y(NO₃)₃·6H₂O was used instead of dysprosium(III). Yield: 72.3%. Anal. Calcd for C₃₄H₇₀Co₂YF₆O₁₈P₇: C, 31.30; H, 5.41. Found: C, 31.38; H, 5.49.

[Dy(L_{OEt})₂](PF₆) Diluted 20-fold with [Y(L_{OEt})₂](PF₆) (diluted-**1**). An aqueous solution (2 mL) of Dy(NO₃)₃·5H₂O (0.005 mmol) and Y(NO₃)₃·6H₂O (0.10 mmol) was added to a solution of NaL_{OEt} (111.4 mg, 0.20 mmol) and NH₄PF₆ (32.6 mg, 0.20 mmol) in water (15 mL) with stirring. A yellow precipitate was generated, and the mixture was stirred at room temperature for 12 h. The precipitate was filtered, washed with water, and dried in air. Anal. Calcd for C₇₁₄H₁₄₇₀Co₄₂Y₂₀DyF₁₂₆O₃₇₈P₁₄₇: C, 31.22; H, 5.39. Found: C, 31.33; H, 5.35.

[Dy(L_{OiPr})₂](PF₆) (**2**). Compound **2** was obtained by the same procedure as that for compound **1** except for using NaL_{OiPr} instead of NaL_{OEt}. Yield: 52.7%. Anal. Calcd for C₄₆H₉₄Co₂DyF₆O₁₈P₇: C, 35.77; H, 6.00. Found: C, 35.77; H 6.08.

Physical Measurements. Elemental analyses for carbon, hydrogen, and nitrogen were performed at the Elemental Analysis Service Center of Sogang University. Powder X-ray diffraction data were recorded using Cu K α (λ = 1.5406 Å) on a Rigaku Ultima III diffractometer with a scan speed of 2°/min and a step size of 0.02°. Magnetic susceptibilities for complexes **1** and **2** were carried out using a Quantum Design SQUID susceptometer (direct current) and a PPMS magnetometer (alternating current, ac). Diamagnetic corrections of all samples were estimated from Pascal's tables.

Crystallographic Structure Determination. X-ray data for **1** and **2** were collected on a Bruker SMART APEXII diffractometer equipped with graphite-monochromated Mo K α radiation (λ = 0.71073 Å). A preliminary orientation matrix and cell parameters were determined from three sets of ϕ scans at different starting angles. Data frames were obtained at scan intervals of 0.5° with an exposure time of 10 s/frame. The reflection data were corrected for Lorentz and polarization factors. Absorption corrections were carried out using SADABS. The structures were solved by direct methods and refined by full-matrix least-squares analysis using anisotropic thermal parameters for non-hydrogen atoms with the SHELXTL program. In complex **2**, the Cp ring and diisopropylphosphito groups were disordered over two sites (0.61 and 0.39 for parts A and B, respectively) using PART, and the isopropoxy groups were isotropically refined. All hydrogen atoms were calculated at idealized positions and refined with the riding models. The crystal data for **1** and **2** are summarized in Table S1.

Computational Details. The electronic structures of **1** and **2** were determined using the CONDON computational package.¹⁶ As the starting point, we used the crystal-field parameters (CFPs) determined by the REC model¹⁷ using the SIMPRE computational package¹⁸ and assuming an ideal D_{3d} coordination environment with the C₃ axis oriented in the z direction. Then, the magnetic properties of **1** were fitted using the full Hamiltonian. The resulting CFPs were tested with the prediction of the experimental single-crystal magnetic anisotropy measurements. Because of the chemical and structural similarity of **2**, the set of CFPs determined for **1** were used as input to fit the magnetic properties of **2**. The free-ion parameters of dysprosium introduced in CONDON (electron repulsion parameters F^k (k = 2, 4, 6) and spin-orbit coupling constant ξ_{SO}) were not varied during the fitting procedures.

RESULTS AND DISCUSSION

Description of the Structures. To design the complexes, we chose the tripodal ligands [CpCo{P(O)(OR)₂}₃][−] (Figure S1), here shortened to L_{OR}[−] (R = Et, iPr), because huge steric encumbrance is fundamental to hindering the tendency of rare earths to move to higher coordination numbers (synthesis in the experimental section). Both [Dy(L_{OR})₂]⁺ complexes crystallize in the monoclinic space group C2/c, with a PF₆[−] anion (Figure 1).

The dysprosium atom is sandwiched between six oxygen atoms from two L_{OR}[−] ligands, successfully forming the planned hexacoordinated structure. The Dy–O bond lengths are very homogeneous, ranging between 2.249 and 2.257 Å for **1** and between 2.246 and 2.265 Å for **2**. The angular deviation parameter, defined as the sum of the deviation from 90° of the 12 cis angles in the coordination sphere, is estimated to be Σ = 90.9° for **1** and 71.6° for **2**.¹⁹ The shape-deviation parameters S_X against an ideal octahedron (X = O) and a trigonal prism (X = P) provide S_O = 1.66 and S_P = 8.95 for **1** and S_O = 0.52 and S_P = 15.11 for **2**, showing that continuous-shape measures²⁰ clearly indicate an octahedral geometry. While a perfect octahedron is obtained in **2**, the use of different L_{OR}[−] ligands allows distortion of the octahedron, producing a twisting angle in **1** (Figure 1b,d). The diamagnetic CpCo and PF₆[−] parts are positioned among the molecules and magnetically shield them, where the shortest Dy–Dy distance is 12.1 Å for **1** and 12.7 Å for **2** (Figures S2 and S3).

Magnetic Properties. The magnetic susceptibilities χ_m of **1** and **2** (i.e., the ratio M/H between the magnetization M and the magnetic field H) were measured at H = 1 kOe down to 2.0 K (Figures S5 and S6). The $\chi_m T$ values at room temperature for **1** and **2** are 13.5 and 13.7 cm³ K mol^{−1}, respectively, close to the 14.2 cm³ K mol^{−1} value expected for the ⁶H_{15/2} state of dysprosium(III). $\chi_m T$ first decreases gradually with T and plummets abruptly below 40 K because of depopulation of the

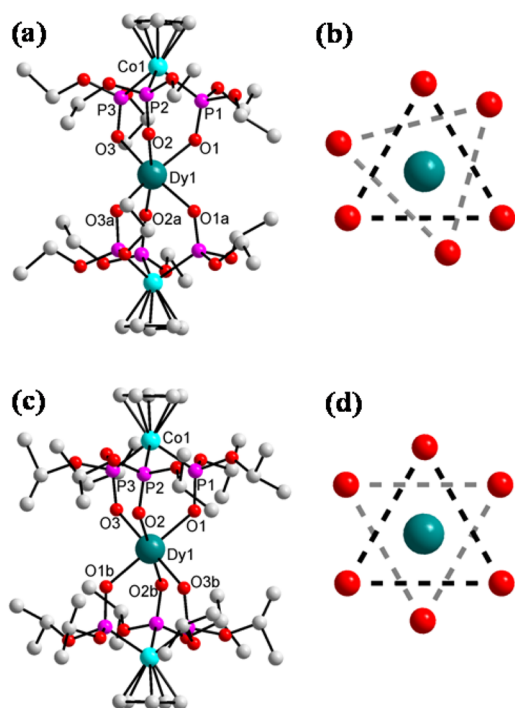


Figure 1. View of the crystal structure of (a) the cationic part of **1**, (b) its dysprosium coordination environment, (c) the cationic part of **2**, and (d) its dysprosium coordination environment. Hydrogen atoms are omitted for clarity.

relaxation time τ becomes slower, reaches a peak (at $H_p = 600$ and 750 Oe for **1** and **2**), and then decreases rapidly, as expected for the progressive suppression of quantum tunneling by H . Both **1** and **2** show a frequency-dependent peak in χ_m'' versus T , and τ was extracted by fitting the ac curves with a Debye model. The resulting Arrhenius plot shows a linear region at high T and a marked kink at lower T , indicating the presence of a thermally activated mechanism still competing with quantum tunneling.

In order to avoid overparameterization, we fit the ac magnetometry data considering either Raman together with quantum-tunneling processes (Figure S24) or a simple Orbach-only process (Arrhenius plot), as expressed by the following equation:

$$\tau = \tau_0 \exp(U_{\text{eff}}/kT)$$

The fit resulted in $\tau_0 = 2.4(5) \times 10^{-8}$ s and $\Delta E = 18(2)$ cm^{-1} for **1** and $\tau_0 = 6.4(5) \times 10^{-7}$ s and $\Delta E = 9(1)$ cm^{-1} for **2** (Figure 3). Both τ_0 values are compatible with SMM behavior,

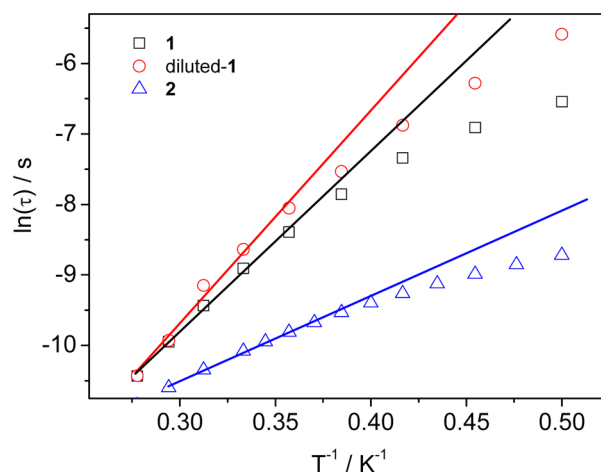


Figure 3. Dynamics of the magnetization as extracted from ac susceptibility measurements for **1** (black squares), **2** (blue triangles), and **1** diluted in a diamagnetic yttrium(III) matrix (red circles). The solid lines represent fits from the Arrhenius formula. For a Raman fit of **1**, see Figure S24.

and fitting of the Argand plots (Figures S13 and S18) shows a narrow distribution of relaxation times, with the spreading parameter $\alpha = 0.2$ and 0.1 for **1** and **2**, respectively. Doping with yttrium(III) produces a very similar dynamic behavior, with a slight decrease of H_p to 450 Oe, and longer τ values. The resulting Arrhenius fit provides $\tau_0 = 6.0(6) \times 10^{-9}$ s and $\Delta E = 21(2)$ cm^{-1} . The spin-flip attempt rate roughly matches the expected value for spin-phonon processes and a barrier at the limits of the extraction errors.

As seen in Figure 3, a simple Arrhenius plot does not capture all of the physics in this system. Raman processes seem to be dominant in the case of **1**, where a satisfactory fit can be obtained for $n = 9$ (Figure S24). The n values of **1** and diluted-**1** are close to 9 , consistent with the parameters obtained from the fitting with an additional Orbach process. However, the Raman model fails for **2**. When n is fixed to 9 , the fit of **2** is poor.

Single-Ion Anisotropy. We now examine the role of the pseudoaxial local environment of the dysprosium(III) octahedron in the anisotropy (Figures S25–S30). Because, in **1**, the dysprosium center is located on a C_2 rotation axis of the $C2/c$ space group, the molecular susceptibility tensor χ must coincide

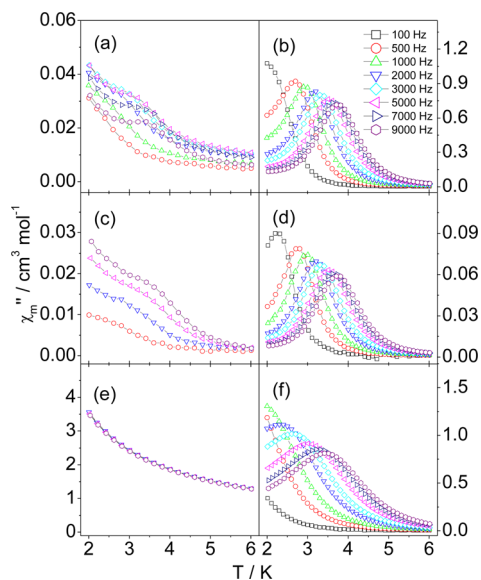


Figure 2. Temperature dependence of the out-of-phase component of the ac magnetic susceptibility, χ_m'' , in zero external field for (a) **1**, (c) diluted-**1**, and (e) **2** and in the external field H_p where the relaxation is slowest for (b) **1**, $H_p = 600$ Oe, (d) diluted-**1**, $H_p = 450$ Oe, and (f) **2**, $H_p = 750$ Oe.

with the crystal one, and it is possible to obtain full magnetic anisotropy by rotating around three orthogonal axes in the low- H limit (Figure 4a). By a fitting and diagonalization procedure,

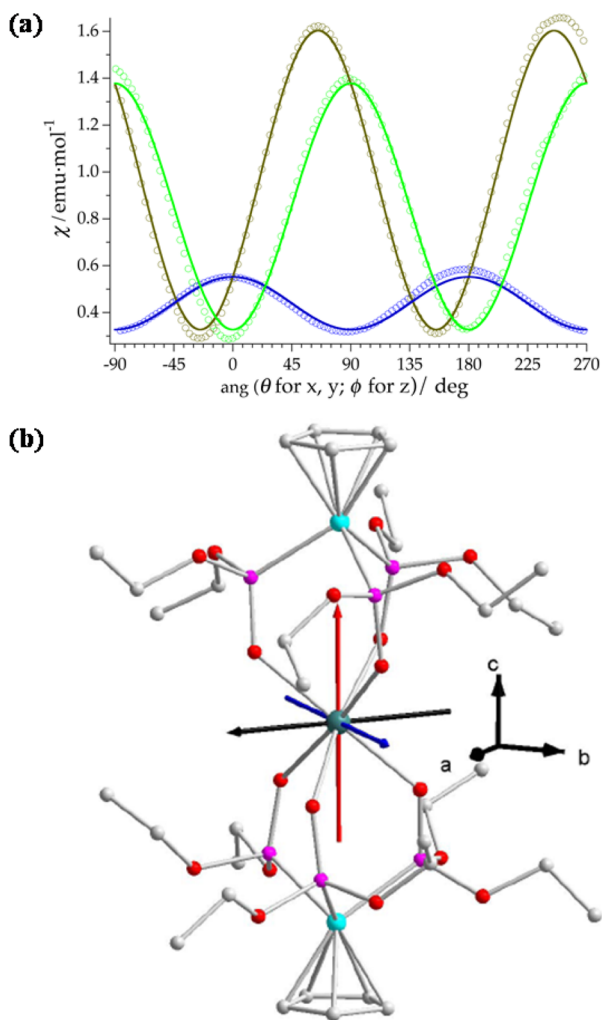


Figure 4. (a) Angular dependence of the magnetic susceptibility of **1** at 11 K. The solid lines are the results of theoretical calculations. (b) Molecular structure showing the easy-axis direction determined from the experiment for an easy axis (red), a medium axis (blue), and a hard axis (black).

we obtain the orientation and magnitude of the principal axes at different T values. One eigenvalue is always dominant, with very prominent easy-axis anisotropy oriented along the pseudo- C_3 molecular axis (Co–Co direction; Figure 4b). This reveals a clean example of uniaxial behavior, consistent with expectations from the theory of octahedral transition-metal ions and without the problems associated with higher-coordination systems. For **2**, the same procedure is not possible because the crystal symmetry prevents direct extraction of the molecular susceptibility.

Theoretical Calculations. The crystallographic coordinates of the first coordination sphere of **1** were idealized in order to reduce the number of non-negligible CFPs. The molecule was oriented with the pseudo- C_3 main axis pointing in the z direction. The idealization of the coordinates resulted in two alternating equilateral triangles of point charges equidistant with respect to the dysprosium ion (~ 2.25 Å). An initial individual fit of the powder magnetic susceptibility data using

the REC model was performed, obtaining the following initial set of CFPs in Wybourne notation (cm^{-1}): $B_{20} = 415$; $B_{40} = -2066$; $B_{43} = 2070$; $B_{60} = 432$; $B_{63} = 2060$; $B_{66} = 702$. They were entered as input in the CONDON package, and only two iterations were needed to obtain a very satisfactory fit (SQX = 0.81%; Figure S5), resulting in the following set of CFPs in Wybourne notation (cm^{-1}): $B_{20} = 559(84)$; $B_{40} = -3300(283)$; $B_{43} = 1693(51)$; $B_{60} = 450(73)$; $B_{63} = 2034(96)$; $B_{66} = 718(342)$. Magnetization at 4, 5, and 6 K was also reproduced (Figure S7). According to this description, the first excited Kramers doublet is found at 32 cm^{-1} , and the total crystal-field splitting of the ground-state J is about 950 cm^{-1} . The energy-level distribution of the ground-state J and the corresponding wave functions are reported in Table S3. The lowest-energy doublet from the next multiplet is located 2668 cm^{-1} above in energy, placed at $\sim 3618 \text{ cm}^{-1}$. The ground-state Kramers doublet in the easy-axis orientation is described by 89.6% of $|\pm^{11/2}\rangle$ with a 9.4% contribution of $|\pm^5/2\rangle$, which corresponds to an effective g_{\parallel} of 13.74 [$g_{\parallel}(\text{exp}) = 13.83$] and $g_{\perp} = 0.48$. This description is almost in perfect agreement with the observed easy-axis behavior (Figure S29). Thus, the angular dependence of the susceptibility of **1** is also reproduced accurately (Figures S31–S33), validating once more the theoretical results. Also, because of the chemical similarity and similar coordination environment of **2**, we have used the calculated set of CFPs as the starting point to model the magnetic susceptibility of **2**. An excellent agreement with SQX = 0.69% (Figure S6) was achieved with the following set of CFPs in cm^{-1} : $B_{20} = 467(301)$; $B_{40} = -3605(990)$; $B_{43} = 596(215)$; $B_{60} = 164(133)$; $B_{63} = 1545(281)$; $B_{66} = -357(2489)$, reproducing also magnetization curves (Figure S8). The uncertainties estimated for the CFPs are reported in Table S2. The large uncertainties found in some of the CFPs likely stem from the sole consideration of the powder magnetic susceptibility data; i.e., single-crystal data were not taken into account. One should consider these uncertainties as an upper limit because (1) we introduced structural information as a starting point and (2) we are predicting instead of fitting the magnetic anisotropy experimental data. The energy-level scheme of the ground-state multiplet and the microstate contributions to the wave functions are also reported in Table S3. The first excited-state doublet is placed at about 44 cm^{-1} , and the total splitting is $\sim 853 \text{ cm}^{-1}$. In this case, the ground-state wave function is more pure, being determined by 98.4% of $|\pm^{11/2}\rangle$ according to our calculations. This leads to a slightly larger value of g_{\parallel} (14.54) compared with that of **1** (13.74). Nevertheless, this subtle difference would need a finer determination by spectroscopic measurements.

In square-antiprismatic systems, the dynamics depend on the axial compression or elongation of the complex, and the presence of a twist angle lowers the barrier and introduces additional transverse terms that favor quantum tunneling. We now use an electrostatic model to reproduce the observations and study structure–property correlations. The states of rare earths are, in general, a linear combination of pure $|m_j\rangle$ spin sublevels, with mixing introduced by the high spin–orbit coupling and the symmetry of the system. In ligand-field theory, the orientation of the quantization axis depends only on the distribution of the charges around the spin. By expanding the electron density of the $|m_j\rangle$ states into a series of spherical harmonics Y_k^0 (with $k \leq 6$),²⁵ we can calculate the potential energy of each pure $|m_j\rangle$ state as a function of the orientation, so as to find the resulting preferred orientation of the easy axis.⁷

The results obtained considering the charges inside **1** and **2** are plotted in Figure 5a,b against the azimuthal φ and polar θ

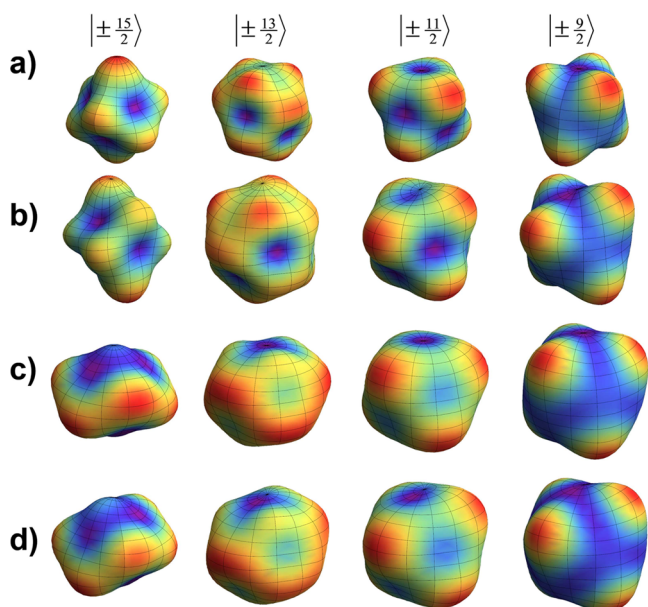


Figure 5. Potential energy surfaces, represented in spherical coordinates, for the different orientations of the pure $|m_j\rangle$ spin sublevels (only the highest four displayed) for (a) **1** and (b) **2**. The same plots for **1** (c) and **2** (d) were obtained by removing the positively charged and diamagnetic cobalt(III) ions. The colorscale indicates the energy (violet, lowest; red, highest), and the vertical position is along the pseudo- C_3 axis.

angles of the spherical coordinates. From the results, it is evident that, for **1**, both the $|^{11/2}\rangle$ and $|^9/2\rangle$ states have an absolute energy minimum at $\theta = 0$, which corresponds to the direction of the pseudo- C_3 molecular axis. They must thus be the dominant contribution to stabilize the observed orientation of the magnetization easy axis. This is in perfect agreement with the phenomenological fit by CONDON for both complexes. On the contrary, the highest m_j state, $|^{15/2}\rangle$, often assumed as the dominant ground-state contribution in rare-earth SMMs, stabilizes a tilted easy axis. A more regular octahedral geometry, as observed in passing from **1** to **2**, changes the preferred easy-axis orientation of the $|^{11/2}\rangle$ contribution, moving it to a transverse geometry and predictably lowering the barrier. According to these calculations, the diamagnetic cobalt(III) ions are revealed to be surprisingly important in **1** because they provide a strong positive charge along the pseudo- C_3 axis. This is fundamental in reducing the $|^{15/2}\rangle$ contribution to the ground state because the highest m_j state is predicted to be preferentially oriented where the negative charge is most dense. Without the cobalt(III) ions, the coordinating atoms and Cp^- rings would stabilize a $|^{15/2}\rangle$ ground state (Figures 5c,d and S34 and S35).

CONCLUSIONS

We have rationally used bulky tripodal ligands to obtain a nearly ideal octahedral geometry around rare earths, resulting in two new dysprosium(III) SMMs. We have subjected them to a detailed experimental and theoretical magnetic analysis. When the REC model (an effective point-charge approach) and the CONDON software (using the full Hamiltonian) are combined, it has been possible to theoretically simulate the

magnetic anisotropy, including the susceptibility along three perpendicular rotations. Furthermore, using these considerations, we could rationalize the role of the different constituents of the molecule, including the diamagnetic cobalt(III) ions, which provide a strong positive charge along the pseudo- C_3 axis, making it the main magnetic axis in spite of the near-octahedral coordination sphere.

ASSOCIATED CONTENT

Supporting Information

The Supporting Information is available free of charge on the ACS Publications website at DOI: 10.1021/acs.inorgchem.6b03118.

Additional structural and magnetic data for the complexes (PDF)

X-ray crystallographic file in CIF format for **1** (CIF)

X-ray crystallographic file in CIF format for **2** (CIF)

AUTHOR INFORMATION

Corresponding Authors

*E-mail: alejandro.gaita@uv.es.

*E-mail: lapo.bogani@materials.ox.ac.uk.

*E-mail: cshong@korea.ac.kr.

ORCID

ShangDa Jiang: 0000-0003-0204-9601

Alejandro Gaita-Ariño: 0000-0002-1600-8627

Chang Seop Hong: 0000-0002-4329-4745

Author Contributions

The manuscript was written through contributions of all authors. All authors have given approval to the final version of the manuscript. These authors contributed equally.

Notes

The authors declare no competing financial interest.

ACKNOWLEDGMENTS

We are thankful for financial support from the Korean Basic Science Research Program (NRF-2015R1A2A1A10055658), an KCRC grant (Grant NRF-2012-0008901), the Korean Priority Research Centers Program (NRF2010-0020209), EU (ERC-CoG-647301 DECRESIM, ERC-StG-338258 OptoQMol, and COST Action 15128 MOLSPIN), the Spanish MINECO (Grant MAT2014-56143-R, CTQ2014-52758-P and Excellence Unit María de Maeztu MDM-2015-0538), and the Generalitat Valenciana (Prometeo Programme of excellence). A.G.-A. acknowledges funding by the MINECO (Ramón y Cajal contract).

REFERENCES

- (1) (a) Ishikawa, N.; Sugita, M.; Ishikawa, T.; Koshihara, S.-y.; Kaizu, Y. Lanthanide Double-Decker Complexes Functioning as Magnets at the Single-Molecular Level. *J. Am. Chem. Soc.* **2003**, *125*, 8694–8695. (b) Ishikawa, N.; Sugita, M.; Ishikawa, T.; Koshihara, S.-y.; Kaizu, Y. Mononuclear Lanthanide Complexes with a Long Magnetization Relaxation Time at High Temperatures: A New Category of Magnets at the Single-Molecular Level. *J. Phys. Chem. B* **2004**, *108*, 11265–11271.
- (2) (a) Woodruff, D. N.; Winpenny, R. E.; Layfield, R. A. Lanthanide single-molecule magnets. *Chem. Rev.* **2013**, *113* (7), 5110–5148. (b) Liddle, S. T.; van Slageren, J. Improving f-element single molecule magnets. *Chem. Soc. Rev.* **2015**, *44* (19), 6655–6669. (c) Gregson, M.; Chilton, N. F.; Ariciu, A.-M.; Tuna, F.; Crowe, I. F.; Lewis, W.; Blake, A. J.; Collison, D.; McInnes, E. J. L.; Winpenny, R. E. P.; Liddle, S. T.

- 401 A monometallic lanthanide bis(methanediide) single molecule magnet
402 with a large energy barrier and complex spin relaxation behavior.
403 *Chem. Sci.* **2016**, 7 (1), 155–165. (d) Chen, Y. C.; Liu, J. L.; Ungur, L.;
404 Liu, J.; Li, Q. W.; Wang, L. F.; Ni, Z. P.; Chibotaru, L. F.; Chen, X. M.;
405 Tong, M. L. Symmetry-Supported Magnetic Blocking at 20 K in
406 Pentagonal Bipyramidal Dy(III) Single-Ion Magnets. *J. Am. Chem. Soc.*
407 **2016**, 138 (8), 2829–2837. (e) Liu, J.; Chen, Y. C.; Liu, J. L.; Vieru,
408 V.; Ungur, L.; Jia, J. H.; Chibotaru, L. F.; Lan, Y.; Wernsdorfer, W.;
409 Gao, S.; Chen, X. M.; Tong, M. L. A Stable Pentagonal Bipyramidal
410 Dy(III) Single-Ion Magnet with a Record Magnetization Reversal
411 Barrier over 1000 K. *J. Am. Chem. Soc.* **2016**, 138 (16), 5441–5450.
412 (f) Coutinho, J. T.; Antunes, M. A.; Pereira, L. C.; Bolvin, H.; Marcalo,
413 J.; Mazzanti, M.; Almeida, M. Single-ion magnet behavior in
414 $[U(Tp(Me_2))_2]_2$. *Dalton Trans.* **2012**, 41 (44), 13568–13571.
- 415 (3) (a) Martínez-Pérez, M. J.; Cardona-Serra, S.; Schlegel, C.; Moro,
416 F.; Alonso, P. J.; Prima-García, H.; Clemente-Juan, J. M.; Evangelisti,
417 M.; Gaita-Ariño, A.; Sesé, J.; van Slageren, J.; Coronado, E.; Luis, F.
418 Gd-based single-ion magnets with tunable magnetic anisotropy:
419 molecular design of spin qubits. *Phys. Rev. Lett.* **2012**, 108 (24),
420 247213. (b) Luis, F.; Repollés, A.; Martínez-Pérez, M. J.; Aguilà, D.;
421 Roubeau, O.; Zueco, D.; Alonso, P. J.; Evangelisti, M.; Camón, A.;
422 Sesé, J.; Barrios, L. A.; Aromí, G. Molecular prototypes for spin-based
423 CNOT and SWAP quantum gates. *Phys. Rev. Lett.* **2011**, 107 (11),
424 117203. (c) Baldoví, J. J.; Cardona-Serra, S.; Clemente-Juan, J. M.;
425 Coronado, E.; Gaita-Ariño, A.; Prima-García, H. Coherent manipu-
426 lation of spin qubits based on polyoxometalates: the case of the single
427 ion magnet $[GdW_{30}P_5O_{110}]_{14}$. *Chem. Commun.* **2013**, 49 (79), 8922–
428 8924. (d) Baldoví, J. J.; Cardona-Serra, S.; Clemente-Juan, J. M.;
429 Coronado, E.; Gaita-Ariño, A.; Palii, A. Rational design of single-ion
430 magnets and spin qubits based on mononuclear lanthanoid complexes.
431 *Inorg. Chem.* **2012**, 51 (22), 12565–12574. (e) Thiele, S.; Balestro, F.;
432 Ballou, R.; Klyatskaya, S.; Ruben, M.; Wernsdorfer, W. Electrically
433 driven nuclear spin resonance in single-molecule magnets. *Science*
434 **2014**, 344 (6188), 1135–1138.
- 435 (4) (a) Ding, Y.-S.; Chilton, N. F.; Winpenny, R. E. P.; Zheng, Y.-Z.
436 On Approaching the Limit of Molecular Magnetic Anisotropy: A Near-
437 Perfect Pentagonal Bipyramidal Dysprosium(III) Single-Molecule
438 Magnet. *Angew. Chem., Int. Ed.* **2016**, 55, 16071–16074. (b) Zadrozny,
439 J. M.; Niklas, J.; Poluektov, O. G.; Freedman, D. E. Millisecond
440 Coherence Time in a Tunable Molecular Electronic Spin Qubit. *ACS*
441 *Cent. Sci.* **2015**, 1 (9), 488–492.
- 442 (5) (a) Atzori, M.; Morra, E.; Tesi, L.; Albino, A.; Chiesa, M.; Sorace,
443 L.; Sessoli, R. Quantum Coherence Times Enhancement in
444 Vanadium(IV)-based Potential Molecular Qubits: the Key Role of
445 the Vanadyl Moiety. *J. Am. Chem. Soc.* **2016**, 138 (35), 11234–11244.
446 (b) Lunghi, A.; Totti, F.; Sessoli, R.; Sanvito, S. The role of
447 anharmonic phonons in under-barrier spin relaxation of single
448 molecule magnets. *Nat. Commun.* **2017**, 8, 14620. (c) Escalera-
449 Moreno, L.; Saud, N.; Gaita-Ariño, A.; Coronado, E. Determining
450 Key Local Vibrations in the Relaxation of Molecular Spin Qubits and
451 Single Molecule Magnets. *J. Phys. Chem. Lett.* **2017**, 8, 1695.
- 452 (6) (a) Clemente-Juan, J. M.; Coronado, E.; Gaita-Ariño, A.
453 Magnetic polyoxometalates: from molecular magnetism to molecular
454 spintronics and quantum computing. *Chem. Soc. Rev.* **2012**, 41 (22),
455 7464–7478. (b) Cardona-Serra, S.; Clemente-Juan, J. M.; Coronado,
456 E.; Gaita-Ariño, A.; Camón, A.; Evangelisti, M.; Luis, F.; Martínez-
457 Pérez, M. J.; Sesé, J. Lanthanoid single-ion magnets based on
458 polyoxometalates with a 5-fold symmetry: the series $[LnP_5W_{30}O_{110}]^{12-}$
459 ($Ln^{3+} = Tb, Dy, Ho, Er, Tm, \text{ and } Yb$). *J. Am. Chem. Soc.* **2012**, 134
460 (36), 14982–14990.
- 461 (7) Chilton, N. F.; Collison, D.; McInnes, E. J.; Winpenny, R. E.;
462 Soncini, A. An electrostatic model for the determination of magnetic
463 anisotropy in dysprosium complexes. *Nat. Commun.* **2013**, 4, 2551.
- 464 (8) (a) Zhang, P.; Guo, Y.-N.; Tang, J. Recent advances in
465 dysprosium-based single molecule magnets: Structural overview and
466 synthetic strategies. *Coord. Chem. Rev.* **2013**, 257 (11–12), 1728–
467 1763. (b) Qian, K.; Baldoví, J. J.; Jiang, S.-D.; Gaita-Ariño, A.; Zhang,
468 Y.-Q.; Overgaard, J.; Wang, B.-W.; Coronado, E.; Gao, S. Does the
thermal evolution of molecular structures critically affect the magnetic
anisotropy? *Chem. Sci.* **2015**, 6 (8), 4587–4593.
- (9) (a) Jiang, S. D.; Wang, B. W.; Su, G.; Wang, Z. M.; Gao, S. A
mononuclear dysprosium complex featuring single-molecule-magnet
behavior. *Angew. Chem., Int. Ed.* **2010**, 49 (41), 7448–7451. (b) Bi, Y.;
Guo, Y. N.; Zhao, L.; Guo, Y.; Lin, S. Y.; Jiang, S. D.; Tang, J.; Wang,
B. W.; Gao, S. Capping ligand perturbed slow magnetic relaxation in
dysprosium single-ion magnets. *Chem. - Eur. J.* **2011**, 17 (44), 12476–
124781. (c) Li, D. P.; Wang, T. W.; Li, C. H.; Liu, D. S.; Li, Y. Z.; You,
X. Z. Single-ion magnets based on mononuclear lanthanide complexes
with chiral Schiff base ligands $[Ln(FTA)_3L]$ ($Ln = Sm, Eu, Gd, Tb$ and
Dy). *Chem. Commun.* **2010**, 46 (17), 2929–2931. (d) Wang, H.;
Wang, K.; Tao, J.; Jiang, J. Twist angle perturbation on mixed
(phthalocyaninato)(porphyrinato) dysprosium(III) double-decker
SMMs. *Chem. Commun.* **2012**, 48 (24), 2973–2975. (e) Chen, G. J.;
Guo, Y. N.; Tian, J. L.; Tang, J.; Gu, W.; Liu, X.; Yan, S. P.; Cheng, P.;
Liao, D. Z. Enhancing anisotropy barriers of dysprosium(III) single-
ion magnets. *Chem. - Eur. J.* **2012**, 18 (9), 2484–2487.
- (10) Baldoví, J. J.; Rosaleny, L. E.; Ramachandran, V.; Christian, J.;
Dalal, N. S.; Clemente-Juan, J. M.; Yang, P.; Kortz, U.; Gaita-Ariño, A.;
Coronado, E. Molecular spin qubits based on lanthanide ions
encapsulated in cubic polyoxopalladates: design criteria to enhance
quantum coherence. *Inorg. Chem. Front.* **2015**, 2, 893–897.
- (11) Shiddiq, M.; Komijani, D.; Duan, Y.; Gaita-Ariño, A.; Coronado,
E.; Hill, S. Enhancing coherence in molecular spin qubits via atomic
clock transitions. *Nature* **2016**, 531, 348–351.
- (12) Jenkins, M. D.; Duan, Y.; Diosdado, B.; García-Ripoll, J. H.;
Gaita-Ariño, A.; Giménez-Saiz, C.; Alonso, P. J.; Coronado, E.; Luis, F.
Coherent manipulation of three-qubit states in a molecular single-ion
magnet. *Phys. Rev. B: Condens. Matter Mater. Phys.* **2017**, 95, 064423.
- (13) Liu, J.-L.; Chen, Y.-C.; Zheng, Y.-Z.; Lin, W.-Q.; Ungur, L.;
Wernsdorfer, W.; Chibotaru, L. F.; Tong, M.-L. Switching the
anisotropy barrier of a single-ion magnet by symmetry change from
quasi- D_{3h} to quasi- O_h . *Chem. Sci.* **2013**, 4, 3310–3316.
- (14) (a) Zeng, D.; Ren, M.; Bao, S.-S.; Li, L.; Zheng, L.-M. A
luminescent heptanuclear $DyIr_6$ complex showing field-induced slow
magnetization relaxation. *Chem. Commun.* **2014**, 50, 8356–8359.
(b) König, S. N.; Chilton, N. F.; Maichle-Mössmer, C.; Pineda, E. M.;
Pugh, T.; Anwender, R.; Layfield, R. A. Fast magnetic relaxation in an
octahedral dysprosium tetramethyl-aluminate complex. *Dalton Trans.*
2014, 43, 3035–3038. (c) Klementyeva, S. V.; Afonin, M. Y.;
Bogomyakov, A. S.; Gamer, M. T.; Roesky, P. W.; Konchenko, S. K.
Mono- and Dinuclear Rare-Earth Chlorides Ligated by a MesitylOSub-
stituted β -Diketiminato. *Eur. J. Inorg. Chem.* **2016**, 2016, 3666–3672.
- (15) (a) Kläui, W.; Eberspach, W.; Güttlich, P. Spin-Crossover Cobalt
(III) Complexes: Steric and Electronic Control of Spin State. *Inorg.*
Chem. **1987**, 26, 3977–3982. (b) Kläui, W.; Eberspach, W.; Schwarz,
R. ZUR REAKTIVITÄT VON COBALTOCEN UND NICKEL-
OCEN GEGENÜBER SEKUNDÄREN PHOSPHINCHALKOGE-
NIDEN: EIN WEG ZU MEHRZÄHNIGEN SAUERSTOFF-UND
SCHWEFEL-LIGANDEN. *J. Organomet. Chem.* **1983**, 252, 347–357.
- (16) (a) van Leusen, J.; Speldrich, M.; Schilder, H.; Kögerler, P.
Comprehensive insight into molecular magnetism via CONDON: Full
vs. effective models. *Coord. Chem. Rev.* **2015**, 289–290, 137–148.
(b) Speldrich, M.; Schilder, H.; Lueken, H.; Kögerler, P. A
Computational Framework for Magnetic Polyoxometalates and
Molecular Spin Structures: CONDON 2.0. *Isr. J. Chem.* **2011**, 51,
215–227.
- (17) Baldoví, J. J.; Borrás-Almenar, J. J.; Clemente-Juan, J. M.;
Coronado, E.; Gaita-Ariño, A. Modeling the properties of lanthanoid
single-ion magnets using an effective point-charge approach. *Dalton*
Trans. **2012**, 41 (44), 13705–13710.
- (18) Baldoví, J. J.; Cardona-Serra, S.; Clemente-Juan, J. M.;
Coronado, E.; Gaita-Ariño, A.; Palii, A. SIMPRE: A software package
to calculate crystal field parameters, energy levels, and magnetic
properties on mononuclear lanthanoid complexes based on charge
distributions. *J. Comput. Chem.* **2013**, 34 (22), 1961–1967.

- (19) Drew, M. G. B.; Harding, C. J.; McKee, V.; Morgan, G. G.; Nelson, J. Geometric Control of Manganese Redox State. *J. Chem. Soc., Chem. Commun.* **1995**, 1035–1038.
- (20) Alvarez, S.; Alemany, P.; Casanova, D.; Cirera, J.; Llunell, M.; Avnir, D. Shape maps and polyhedral interconversion paths in transition metal chemistry. *Coord. Chem. Rev.* **2005**, 249 (17–18), 1693–1708.
- (21) (a) Sutter, J.-P.; Kahn, M. L.; Kahn, O. Conclusive Demonstration of the Ferromagnetic Nature of the Interaction Between Holmium(III) and Aminoxy Radicals. *Adv. Mater.* **1999**, 11, 863–865. (b) Kahn, M. L.; Sutter, J.-P.; Golhen, S.; Guionneau, P.; Ouahab, L.; Kahn, O.; Chasseau, D. Systematic Investigation of the Nature of The Coupling between a Ln(III) Ion (Ln) Ce(III) to Dy(III) and Its Aminoxy Radical Ligands. Structural and Magnetic Characteristics of a Series of {Ln(organic radical)₂} Compounds and the Related {Ln(Nitrone)₂} Derivatives. *J. Am. Chem. Soc.* **2000**, 122, 3413–3421.
- (22) (a) Tang, J.; Hewitt, I.; Madhu, N. T.; Chastanet, G.; Wernsdorfer, W.; Anson, C. E.; Benelli, C.; Sessoli, R.; Powell, A. K. Dysprosium triangles showing single-molecule magnet behavior of thermally excited spin states. *Angew. Chem., Int. Ed.* **2006**, 45 (11), 1729–1733. (b) Layfield, R. A.; McDouall, J. J.; Sulway, S. A.; Tuna, F.; Collison, D.; Winpenny, R. E. Influence of the N-bridging ligand on magnetic relaxation in an organometallic dysprosium single-molecule magnet. *Chem. - Eur. J.* **2010**, 16 (15), 4442–4446. (c) Gamer, M. T.; Lan, Y.; Roesky, P. W.; Powell, A. K.; Clérac, R. Pentanuclear Dysprosium Hydroxy Cluster Showing Single-Molecule-Magnet Behavior. *Inorg. Chem.* **2008**, 47, 6581–6583. (d) Zheng, Y.-Z.; Lan, Y.; Anson, C. E.; Powell, A. K. Anion-Perturbed Magnetic Slow Relaxation in Planar {Dy₄} Clusters. *Inorg. Chem.* **2008**, 47, 10813–10815.
- (23) (a) Blagg, R. J.; Tuna, F.; McInnes, E. J.; Winpenny, R. E. Pentametallic lanthanide-alkoxide square-based pyramids: high energy barrier for thermal relaxation in a holmium single molecule magnet. *Chem. Commun.* **2011**, 47 (38), 10587–10589. (b) Koo, B. H.; Lim, K. S.; Ryu, D. W.; Lee, W. R.; Koh, E. K.; Hong, C. S. A unique tetranuclear Er(III)₄ cluster exhibiting field-induced single-molecule magnetism. *Chem. Commun.* **2012**, 48 (19), 2519–2521. (c) Sorace, L.; Benelli, C.; Gatteschi, D. Lanthanides in molecular magnetism: old tools in a new field. *Chem. Soc. Rev.* **2011**, 40 (6), 3092–3104. (d) Jiang, S. D.; Wang, B. W.; Sun, H. L.; Wang, Z. M.; Gao, S. An organometallic single-ion magnet. *J. Am. Chem. Soc.* **2011**, 133 (13), 4730–4733. (e) Snyder, J.; Ueland, B. G.; Slusky, J. S.; Karunadasa, H.; Cava, R. J.; Mizel, A.; Schiffer, P. Quantum-classical reentrant relaxation crossover in Dy₂Ti₂O₇ spin ice. *Phys. Rev. Lett.* **2003**, 91 (10), 107201.
- (24) (a) Brown, A. J.; Pinkowicz, D.; Saber, M. R.; Dunbar, K. R. A Trigonal-Pyramidal Erbium(III) Single-Molecule Magnet. *Angew. Chem., Int. Ed.* **2015**, 54 (20), 5864–5868. (b) Meihaus, K. R.; Minasian, S. G.; Lukens, W. W., Jr.; Kozimor, S. A.; Shuh, D. K.; Tylliszczak, T.; Long, J. R. Influence of pyrazolate vs N-heterocyclic carbene ligands on the slow magnetic relaxation of homoleptic trischelate lanthanide(III) and uranium(III) complexes. *J. Am. Chem. Soc.* **2014**, 136 (16), 6056–6068.
- (25) Sievers, J. Asphericity of 4f-Shell in Their Hund's Rule Ground States. *Z. Phys. B: Condens. Matter Quanta* **1982**, 45, 289–296.